HHS Public Access

Author manuscript

Ophthalmology. Author manuscript; available in PMC 2018 March 01.

Published in final edited form as:

Ophthalmology. 2017 March ; 124(3): 359–373. doi:10.1016/j.ophtha.2016.10.022.

Natural History of the Central Structural Abnormalities in Choroideremia: A Prospective Cross-Sectional Study

Tomas S. Aleman, **Grace Han**, **Leona W. Serrano**, **Nicole M. Fuerst**, **Emily S. Charlson**, **Denise J. Pearson**, **Daniel C. Chung**, **Anastasia Traband**, **Wei Pan**, **Gui-shuang Ying**, **Jean Bennett**, **Albert M. Maguire**, and **Jessica I. W. Morgan**

Scheie Eye Institute, Perelman School of Medicine, Department of Ophthalmology, University of Pennsylvania, Philadelphia, Pennsylvania

Abstract

Purpose—To describe in detail the central retinal structure of a large group of patients with Choroideremia (CHM).

Design—prospective, cross-sectional, descriptive study.

Subjects—Patients (*n*=97, age 6-71 years) with CHM and subjects with normal vision (n=44; ages 10-50 years) were included.

Methods—Subjects were examined with spectral domain optical coherence tomography (SD-OCT) and near infrared reflectance imaging. Visual acuity (VA) was measured during their encounter or obtained from recent ophthalmic examinations. Visual thresholds were measured in a subset of patients (n=24) with automated static perimetry within the central regions (±15°) examined with SD-OCT.

Main outcome measures—VA and visual thresholds, total, inner and outer nuclear layer (ONL) thicknesses, and the horizontal extent of the ONL and of the photoreceptor outer segment (POS) interdigitation zone.

Results—Earliest abnormalities in regions with normally appearing RPE were the loss of the POS and EZ zone associated with rod dysfunction. Transition zones (TZs) from relatively preserved retina to severe ONL thinning and inner retinal thickening moved centripetally with age. Most patients (88%) retained VAs better than 20/40 until their fifth decade of life. VA decline coincided with migration of the TZ near the foveal center. There were outer retinal tubulations in degenerated, non-atrophic retina in the majority (69%) of patients. In general, retinal pigment epithelium (RPE) abnormalities paralleled photoreceptor degeneration, although there were

*Corresponding author: Tomas S. Aleman, M.D., Perelman Center for Advanced Medicine, University of Pennsylvania, 3400 Civic Center Boulevard, Philadelphia, PA 19104. Tel: +1 215 614 4100; Fax: +1 215 615 0527, aleman@mail.med.upenn.edu.

Disclosure: None for any of the authors.

This work was presented in part at the Annual Meeting of The Association for Research in Vision and Ophthalmology, Seattle, Washington, May 2016.

regions with detectable but abnormally thin ONL co-localizing with severe RPE depigmentation and choroidal thinning.

Conclusions—Abnormalities of the POS and rod dysfunction are the earliest central abnormalities observed in CHM. Foveal function is relatively preserved until late disease. TZ migration to the foveal center with foveal thinning and structural disorganization heralded central VA loss. The relationships established may help outline the eligibility criteria and outcome measures for clinical trials for CHM.

Graphical abstract

Precis

Photoreceptor outer segment abnormalities associated with rod dysfunction were the earliest abnormalities observed in choroideremia. Migration of transition zones near the foveal center heralded central vision loss.

Keywords

Choroideremia; optical coherence tomography; rods; photoreceptors

INTRODUCTION

Choroideremia (CHM) is an infrequent (prevalence 1:50 000) X-linked recessive form of hereditary retinal degeneration with a distinctive fundus appearance characterized by scalloped chorioretinal changes with visualization of the sclera through a depigmented or non-existent retinal pigment epithelium (RPE) and choroid.[1-3] Patients experience nyctalopia, typically in the second decade of life, followed by progressive constriction of the visual field in early adulthood and loss of their central vision only later in life (after several decades).[4-14]

The disease is caused by mutations in a single gene (*Rab escort protein-1, REP-1*) on chromosome Xq 21.2, which encodes a ubiquitously expressed protein that forms part of the catalytic Rab geranyl-geranyl transferase (RGGTase) II complex.[15-21] In general, most mutations reported to date are thought to lead to loss-of-function of the encoded protein.[22-23] The disease mechanism has not been completely elucidated but may involve impaired vesicular and/or membrane trafficking resulting from deficient geranylgeranylation of Rab27a.[24-27] Recent evidence suggests a systemic role for REP1 in systemic fatty acid metabolism, although it is presently unclear how such abnormalities impact the retina.[28]

Recent success of gene augmentation trials for Leber's congenital amaurosis (LCA) caused by mutations in *RPE65* paved the way for gene therapy initiatives for other retinal degenerative conditions.[29-32] A phase I/II clinical trial for CHM has published encouraging initial results.[33-34] Confirmation of safety and efficacy in these new trials will help establish gene therapy as a treatment approach for CHM and other inherited retinal degenerations.[29,35,36] Although several groups have initiated clinical trials for various inherited retinopathies including CHM (clinicaltrials.gov), there remain gaps in our understanding of their natural history.

In this present study we examined in detail the central retinal structure of a large group of patients with CHM using spectral domain optical coherence tomography (SD-OCT). Quantitative measures of retinal structure and co-localized measures of retinal function were used to explore the sequence of events leading to structural and functional abnormalities in this condition. The findings may help outline the eligibility criteria and/or outcome measures for initial clinical trials for CHM.

METHODS

Ninety-seven patients (ages, 6-71 years, median=39 years) diagnosed with CHM were included in this prospective, cross-sectional study. Unaffected subjects with normal ophthalmic examination (n=44; ages 10-50 years) were also included. Genotyping was undertaken using venous blood samples or, when available, from previous studies. Informed consent was obtained after explanation of the nature of the study; procedures complied with the Declaration of Helsinki and were approved by the institutional review board. Patients had a comprehensive eye examination and best-corrected visual acuity (VA) was measured or was available from recent ophthalmic exams (Supplementary Figure 1; available at http://aaojournal.org). Spectral domain (SD) optical coherence tomography OCT was performed in 92 patients (n=184 eyes) (Spectralis, Heidelberg Engineering, Carlsbad, CA) with 6 or 9 mm-long horizontal sections crossing the anatomical fovea. Segmentation of SD-OCT images was performed with the built-in automatic segmentation software of the Spectralis system. ImageJ imaging analysis software (plot profile analysis feature) (http://imagej.nih.gov/ij/links.html) was used to supervise measurements and ensure correct identification of the different laminar boundaries. Retinal thickness was defined as the distance between the signal transition at the vitreoretinal interface (from the internal limiting membrane, ILM) and the posterior boundary of the major signal corresponding to the basal retinal pigment epithelium (RPE)/Bruch's membrane. In normal subjects, the RPE-Bruch's signal is the last reflectivity within the 4-5 signals that are identifiable in the outer retina. In patients, the presumed RPE signal was sometimes the only signal in the outer retina and often merged with signals from the anterior choroid. The RPE peak intensity was then specified manually by considering the properties of the backscattering signal originating from layers vitread and sclerad to it.[8] The outer nuclear layer (ONL) thickness was defined as the major intraretinal hyporreflective signal bracketed between the outer plexiform layer (OPL) and the external limiting membrane (ELM). The inner retinal thickness was defined as the distance between the ILM and the OPL.[37] The horizontal extent of uninterrupted ONL and the inner segment ellipsoid zone (EZ) layer was determined visually as the distance from the foveal center to the location in nasal or temporal retina at which the layer was no longer visible, which was confirmed, when needed, by inspecting the longitudinal reflectivity profile generated at that location using ImageJ analysis tools. Measurements were performed along a line parallel to the RPE using digital calipers from the SD-OCT software and were expressed as 'total horizontal extent" (temporal+nasal) or as nasal or temporal 'lateral extent', respectively. En-face near infrared reflectance (NIR-REF) images obtained during the acquisition of the OCTs were also available for analysis. The area of preserved RPE melanin by NIR-REF was manually defined using the imaging tools available within the Spectralis system. The software automatically calculates the area within

a given perimeter; scalloped regions of demelanization within areas of apparently better preserved RPE were subtracted from this total. Twenty four patients within this group had light-adapted achromatic and dark-adapted chromatic (500 nm and 650 nm) automated static perimetry (200 ms duration,1.7°diameter stimuli), using a modified Humphrey Field Analyzer (HFA II-i, Carl Zeiss Meditec, Dublin, CA), following published methodology.[38-40] Thresholds were measured along the horizontal meridian at 2° intervals, extending to 30°of eccentricity, corres ponding to the retinal region scanned with SD-OCT.[39,40] Some of these patients (n=12) also had fundus automated perimetry (MAIA, CenterVue Inc., Fremont, CA, USA) with dilated pupils and after 30 minutes of dark-adaption using an achromatic (0.45°in diameter) stimulus an d a 10-2 protocol. A horizontal sensitivity profile was generated by averaging points above and below (±1°) the horizontal meridian for each eccentricity in this standard 10-2 protocol grid. The lateral extent of the field was estimated by determining the eccentricity at which the sensitivity within this interpolated profile was reduced to <5dB.

Statistical analysis

OCT parameters and VA across age groups (<20, 20-40 and >40 years) were compared by using analysis of variance. The inter-eye correlation was accounted for by using the generalized estimating equations (GEE).[41] Linear regression models were used to evaluate the association between age, OCT parameters and VA (in LogMAR), and their association with age was summarized using the slope for each age group, testing if the slope was significantly different from zero. The linear slopes of the two older age groups were compared to the age group of <20 years of age. The inter-ocular agreement of the OCT measurements was assessed using mean inter-ocular differences (IOD). The 95% limit of agreement was estimated as the mean IOD±1.96 standard deviations (SD). The association between the IOD of OCT parameters and age was assessed by comparing linear regressions and mean IOD across different age groups. All statistical analyses were performed in SAS 9.4 (SAS Institute Inc, Cary, NC), and two-sided $p<0.05$ was considered to be statistically significant.

RESULTS

Central Structural Changes in CHM Hemizygotes: From Early to End-Stage Disease

Ninety seven patients with CHM were included in this study. Patients were diagnosed clinically by the characteristic fundus appearance, visual field defects and electroretinography supported in many by a positive family history. Genotyping results were available for 79 of them. Thirty five patients had nonsense mutations; others had frameshift (n=17) and splicing (n=10) mutations leading to a premature stop. Three individuals had missense mutations and 14 had deletions of 2 or more exons of whom five had deletion of the entire gene (Supplementary Table 1; available at http://aaojournal.org). Three of the mutations were novel. Horizontal SD-OCT cross-sections in patients representing different stages of the disease are shown compared to a normal subject (Fig. 1). In the normal subject there is a foveal depression and the retinal laminae are easily discernible with hyporreflective nuclear layers (ONL; inner nuclear layer, INL; ganglion cell layer, GCL), separated by hyperreflective bands that correspond to the OPL and inner plexiform layer

(IPL). The outer boundary of the ONL is delimited by the ELM. Signal bands external to the ELM represent the EZ, the interdigitation zone (IZ) between the photoreceptor outer segment tips and the apical RPE, the RPE, and Bruch's membrane as the posterior boundary of the RPE (Fig. 1). Beyond the RPE/Bruch's membrane (RPE/BM) there are signals originating from the choroidal vasculature, which end at the choroidal-scleral boundary (Fig. 1, *small arrows*). A normal en-face NIR-REF image shows the dark vascular pattern overlying a diffusely homogeneous grayish background that may be slightly darker near the foveal center, especially in young subjects (Fig. 1, *left panels*). Patients representing different disease stages are used to illustrate the natural history of the disease in Fig. 1. A 6-year-old patient with CHM shows increased visualization of the pericentral choroidal vasculature on NIR-REF imaging (Fig. 1, Patient 1, P1), although visualization of choroidal features is possible in otherwise normal subjects.[42] On SD-OCT cross section the overall retinal architecture appears normal. However, closer inspection reveals a transition zone (TZ) (Fig. 1, P1, *vertical arrow*) of attenuation and then loss of the IZ signal in nasal retina with approximation of the EZ to the RPE and mild ONL thinning, consistent with photoreceptor outer segment shortening (POS) and cell loss.[8,10,42-44] Further nasal to this point there is increased backscattering posterior to the RPE/BM. The structural change co-localizes with a transition of the NIR-REF signal from normal to a brighter signal near the nerve (Fig. 1, vertical arrow). By the time patients reach the second decade of life, although POS may be clearly seen within 2 mm of the foveal center, there is usually attenuation or total loss of this signal at greater eccentricities. The lateral extent of the EZ and IZ bands in pericentral retina is variable and loss of the IZ signal appears to occur early in the disease in regions with otherwise apparent normal pigmentation on clinical exam and on en-face NIR-REF imaging (Fig. 1, P2 & P3). In these areas of apparent normal pigmentation the EZ is often seen at the apical RPE without an interposing IZ (Fig. 1, P2). TZs of obvious structural change with EZ loss, severe ONL thinning and increased posterior backscattering co-localize to the edge of clearly depigmented lesions on fundus exam and on NIR-REF, and were already apparent within the central retina (<15° of eccentricity) in all young patients (age ≤15 years) in this study, confirming earlier observations (Fig. 1, P2 & P3).[7,8,10] At the TZ there is an outward evagination of the ELM and EZ layers (Fig. 1, P3, *yellow outline*). Outer retinal tubulations (ORTs; Fig. 1, *asterisks*) were seen a short distance peripherally to the TZ along the horizontal profiles in 69% of the eyes and occurred nearly always within depigmented (but not totally atrophic) regions. Similar high frequency of ORT has been previously reported in CHM.[10] The ONL that separates the ORT from the central TZs and that surrounds this lesion is markedly thin. By the third decade of life centripetal progression of the central retinal disease leads to residual islands of relative normal pigmentation with scalloped perimeters surrounded by depigmented RPE/choroid and a thickened fovea causing an abnormal foveal contour (Fig. 1, P4). The ONL can extend asymmetrically from the center in a region with preservation of the EZ signal and of the RPE melanin on NIR-REF. In all patients the distance between the EZ and the apical RPE, as well as the ONL thickness decreases with increasing eccentricity. Hyporeflective lesions, unlike overt cystoid macular edema, were often seen (83/184 eyes) at the TZs located between the evaginated ELM and EZ and the OPL (Fig. 1, *blue asterisks*). Large central outer retinal schisis was observed in 7/184 eyes in this cohort. Of note, the OPL and a thin hyporreflective ONL can be traced for a considerable distance outside of the TZs, interrupted by ORTs, in

depigmented retina with a markedly thin choroid (Fig. 1, P4 & P5). Foveal thickness at this stage is often thicker than normal erasing the normal foveal depression and intraretinal bridges indicative of foveal remodeling may be observed within this central region of relative anatomical preservation.[8] With disease progression there is further centripetal movement of the TZs, which often occurs asymmetrically with further approximation to the fovea on the nasal side of the fovea than on the temporal edge, in many cases nearly bisecting a then thinned fovea (Fig. 1, P5). Patients at end-stage disease may have a very small island of relatively preserved RPE pigmentation on NIR-REF (Fig. 1, P6). The surrounding retina appears posteriorly displaced and shows replacement of the choroidal structures by a deep, wide, hyperreflective band of posterior backscatter. In regions of severe retinal thinning, tubular hyporreflective structures may be traced within the choroid leading to the basal side of the RPE/BM, which may correspond to large choroidal vessels (Fig.1, P5, nasal to the fovea). Despite the degree of structural disorganization, residual foveal photoreceptors with abnormal outer segments can support fine spatial resolution (VA 20/32) albeit with extremely limited mobility from visual field loss (Fig. 1, P6). Foveal thinning and approximation of the edge of degeneration to the foveal center with loss of the foveal EZ and IZ was associated with the final decline in central vision. In some end-stage eyes, not complicated by macular holes or schisis, very abnormal VA (range 0.6-1.6 logMAR, median=0.97, n=18 eyes), was sustained by parafoveal/perifoveal islands of photoreceptors. Total retinal atrophy with and loss of vision is the end result after the six decade of life (not shown).

The relationship between the retinal structure and co-localized measures of rod and cone function in CHM is illustrated in four patients representing different disease stages (Fig. 2). P7 (age 12) shows normal lamination across most of the scan with the exception of POS shortening and loss of the IZ signal (see normal in Fig. 1 for comparison) in association with mildly abnormal rod and cone function. There is a steep transition at 1.5 mm in nasal retina with loss of the EZ signal followed with increasing eccentricity by ONL thinning, increased posterior backscattering from RPE depigmentation and choroidal thinning associated with vision loss. In the third decade there is degeneration closer to the foveal center (Fig. 2, P8). Rod function is barely detectable but cone function is still near normal over a relatively wide expanse of the central retina. The central island of relative preservation is further reduced in extent in the fourth decade of life (Fig. 2, P9). Rod function is no longer detectable; abnormal cone function is measurable only within 1-2 mm of the foveal center. A very small island of profoundly abnormal cone function is measurable only within a few millimeters of the foveal center in end stage disease supported by small region with detectable ONL (Fig. 2, P10).

Quantitative Structural and Functional Relationships of the Central Retina in CHM

Quantitation of retinal thickness parameters from horizontal cross-sections from all patients confirmed an orderly centripetal progression of the central retinal abnormalities (Fig. 2B). In general, overall central retinal, ONL and inner retinal thicknesses were within normal limits in patients in the first decade of life despite the early POS loss described (Fig. 2, *left panel, blue traces*). Localized retinal and ONL thinning can be seen at the peripheral end of the thickness profiles in some patients. A spectrum of thickness abnormalities is clearly seen by

the second decade of life (Fig. 2B, *left panels, green traces*). There is ONL thinning at eccentricities >2 mm in nearly all patients in this age group associated with a hyperthick inner retina, suggestive of reactive remodeling.[8,39,45] More central retina shows ONL and overall foveal thickening. Patients in the third and fourth decade of life show a centripetal movement of the previous patterns (Fig. 2B; *middle panels*). Thinning of previously thicker than normal locations leads to normal or thinner than normal central retinas. ONL continues to be thicker than normal at the fovea in patients in their 30s, but foveal thinning ensues in most patients by the fifth decade of life. The inner retina remains normal or thick in this age group. With a few exceptions, late stage disease is observed in patients beyond the fifth decade of life with further centripetal movement of the abnormalities. A very thin ONL can be measured only within the central ~1 mm of eccentricity in nearly all patients at this stage; the inner retina in this age group can be within normal limits in thickness (Fig. 2B).

Representative patients illustrate the relationship between the total horizontal extent of the central structural abnormalities and visual sensitivity as measured by fundus perimetry (Fig. 3A). Visual sensitivity mapped to a color scale shows that function, detectable only over a small extent, can be near normal in some patients (Fig. 3 A, P11 & 12) for some of the most centrally located points, declining in sensitivity with increasing eccentricity. A horizontal sensitivity profile generated from the 10-2 grid on microperimetry (Fig. 3A, *top panels*, *blue line*) roughly matches the lateral extent of the ONL (Fig. 3A, *bottom panels*). The horizontal extent of the EZ band corresponds closely to the horizontal extent of vision that is within ~1 log units of normal mean sensitivity; the extent of the ONL thickness profile reached further from the center than the EZ profile (Fig. 3A).

The total horizontal extent of the central ONL declined linearly with age at a rate of ~100 μm (~0.3°) per year (Fig. 3B) (Table 1). ORTs (Fig. 3B, *red circles*) were nearly always visible in extrafoveal central retina of CHM patients in the second to sixth decade of life in regions of obvious RPE depigmentation with detectable but thinned ONL and were not detected in regions of total chorioretinal atrophy. In most patients the ONL extended more into temporal than nasal retina (3102 vs 2586 μm; P<0.001; P<0.001). The mean IOD of the ONL extent was 24 μm with a tendency for greater interocular asymmetry in patients >40 years of age (Fig. 3B,D; Table 2). The rate of decline of the EZ total horizontal extent was also ~100 μm/year, showed similar asymmetry around the foveal center with greater extent in temporal retina (1580 vs. 1194 μm), had greater IOD (288 μm) compared to the ONL extent, and demonstrated the same trend toward increased IOD with age (Fig. 3C,D; Table 2). The increased IOD with age was similar for the nasal and temporal central retina for both the ONL (p=0.36) and EZ (p=0.79) lateral extent (Table 2). The total horizontal extent of the EZ related well with the extent the horizontal sensitivity profiles determined by microperimetry (Fig. 3D). Structural parameters may thus be used to estimate the extent of potentially ‘visual’ retina when proper psychophysical measures of vision need to be corroborated or may not be available.

Foveal Abnormalities in Choroideremia

Horizontal cross-sections through the fovea in six CHM patients illustrate the changes in foveal architecture encountered in this large cohort of CHM patients. Foveal

hyperreflectivities tracking into the inner retina from the IZ with (Fig. 4A, P14) or without (Fig. 4A, P15) interruption of the EZ or IZ were seen in ~10% of eyes with an otherwise normal or thickened fovea. VA remains relatively unaffected in these patients. P16 shows a wider gap in the central EZ and a flattened foveal contour with poor VA. Near the TZ in nasal parafovea there is an interruption of the RPE/BM with posterior displacement of the OPL and INL; a thin ONL can be traced throughout the extent of the scan. In some eyes (8/184), large choroidal vessels could be seen abutting against these areas of RPE/BM interruption and posterior displacement. Despite spatially tight foveal SD-OCT scanning the INL can be seen crossing the foveal center in many patients (Fig. 4, P14 right eye,P15,P16). Idiopathic macular hole is somewhat infrequent in adults before the sixth decade of life, yet 4/184 eyes (2.2%) in this cohort showed macular hole even at a young age (Fig. 4A, P14, left eye), consistent with previous reports in CHM.[46-48] Foveal ORTs (Fig, 4A, P17) were observed in 13% of the eyes in association with foveal thinning and approximation of the TZ to the fovea. The TZ nearly dissected the fovea, usually from the nasal side, in many patients at end stage disease. P18 (Fig, 4A) may represent the most favorable foveal outcome in advanced CHM with a thickened but well-structured fovea with little disruption of the cone outer segment (COS) and no obvious interlaminar bridges despite proximity of the TZs to the foveal center and the limited extent of residual retina. Taken together the findings suggest that significant structural abnormalities at the foveal center can occur ahead of the orderly centripetal progression of the extrafoveal changes, which may ultimately modify the foveal phenotype and vision.

Previous work proposed a disease model consisting of several phases transitioning from early photoreceptor and RPE abnormalities and retinal remodeling, leading to end-stage atrophy.[8] We next asked if such a model of the disease will be represented in this large sample of patients. Foveal thickness expressed as a function of age was normal in all patients younger than 15 years of age (Fig. 4B). The earliest SD-OCT changes consisting of EZ to IZ approximation due to shortening of the POS were likely not present at the fovea at this early stage. Initial signs of abnormality were the emergence of interlaminar bridges (Fig. 4B, *green symbols*) and foveal thickening late in the second decade of life. Foveal thickness returns to the normal range in patients between 30-40 years of age, likely due to underlying thinning of previously thickened foveas, and was thinner than normal in most patients over 40 years of age. The slope of the decline in foveal thickness accelerates with age (Table 1). Foveal ORT (Fig. 4B, *red symbols*) were noticed at or near the foveal center in abnormally thin foveas although they were never observed in severely thinned (<80 μm) foveas. Foveal thickness IODs was more variable with increasing age (Fig. 4B; Table 2). VA remained better than 0.3 logMAR (20/40) in the vast majority of patients (108/175 or 88% of eyes with recorded VA). There is a suggestion of faster rates (~0.05 log MAR/year) of VA loss for ages >40 years (Fig. 4C, Table 1). Similarly, foveal sensitivity measured in a subgroup of patients (n=24) with light-adapted perimetry was within normal limits (normal mean=39±4dB) in the majority (33/45) of eyes tested, becoming abnormally reduced for ages>40 years, declining at a rate of ~2dB/year (data not shown). Of note, there are multiple examples in this cohort of patients and in the literature supporting the possibility of excellent VA in advanced age in CHM. There was also increasing variability in the IOD in VA with older age (Fig. 4C, Table 2).

Is there a relationship between foveal thickness and VA and the proximity of the degeneration to the foveal center as measured by the horizontal extent of the EZ? Foveal thickness plotted as a function of EZ extent did not decline below normal limits until the edge of degeneration was within ~2 mm of the foveal center; from then the fovea thinned ~100 μm per each mm of reduction in EZ extent (Fig. 4D, *left panel, thick diagonal*). VA related well with foveal thickness (Fig. 4D, *middle panel*) as well as with the horizontal extent of the EZ (Fig. 4D; *right panel*) (Supplementary Table 2) (available at http://aaojournal.org). In general, VA loss occurred when foveal ONL became abnormally thin showing signs of remodeling with approximation of the TZ to within ~2 mm (2-4 mm total horizontal extent) of the foveal center. It is important to note, however, that the relationships between VA and these two structural parameters were far from perfect with several examples of severe thinning and reduction in extent of the EZ and relatively preserved VA.

Earliest Structural Change in Choroideremia

Fundus abnormalities in patients younger than 20 years of age ranged from diffuse depigmentation more obvious in nasal retina (Figs. 1 and 2, Fig. 5, P19), to central scalloped depigmentation with visualization of the choroidal vasculature (Fig. 5, P20). There was a normal appearance of the foveal center on NIR-REF in all young patients. The pericentral retina can appear lighter on NIR-REF than the center, which coincided with the loss of the IZ signal in pericentral retina. Regions with obvious depigmentation on funduscopy and NIR-REF co-localized with abrupt transitions in retinal structure with loss of the EZ signal, increased backscattering posterior to the RPE layer (Fig. 5A, *vertical arrows*) and various degrees of ONL and choroidal thinning. Within regions without RPE demelanization by NIR-REF young CHM had an otherwise normal retinal lamination but obvious abnormalities distal to the EZ. There was loss or distortion of the IZ signal in most of the pericentral retina of most young patients with approximation of the EZ band to the RPE strongly suggesting that the earliest structural abnormality in CHM resided at the photoreceptor outer segment and/or IZ.

Cross-sectional observations from all patients from this study showed that the area of preserved RPE within the central retina declines rapidly (~5 mm^2/year) within the first two decades of life following an exponential decay function (RPE area=35.1e-0.04 × age) (Fig. 5B). Unlike other parameters there was less IOD in later disease stages as islands of residual retina constricted (Table 2). The lateral extent of the EZ was tightly correlated (Spearman correlation coefficient=0.93, $P<0.0001$) with the lateral extent of uninterrupted RPE preservation as estimated from NIR-REF, confirming the impression of co-localization between severe outer photoreceptor structural abnormality and RPE demelanization (Fig. 5C). The area of weaker NIR-REF signal within the area of RPE preservation noted before appeared to coincide with regions of EZ preservation but IZ signal/POS loss; this was difficult to accurately quantify with the tools available in this work.

Next we asked if POS abnormalities preceded the RPE demelanization by relating ONL thickness against the distance between the EZ and the IZ signal, which relates to the length of the photoreceptor outer segment. Measurements included only areas with intact EZ and normal appearing NIR-REF (representing normal-appearing RPE melanization) in a

subgroup of ten young (age ≤15 years) patients. ONL thickness and POS length (EZ-to-RPE distance) were expressed as a fraction of normal for each location in the horizontal SD-OCT profile. In total, 14196 locations were evaluated and compared to location-specific normal values. A sizeable proportion of the locations (14.8%) showed significant ONL thinning and POS/loss (Fig 5D, *right bottom quadrant*) whereas nearly half (49.2%) of the locations showed significant POS shortening in locations without obvious RPE demelanization or ONL thinning (Fig 5D, right top quadrant), suggesting abnormalities at the POS and/or outer segment-apical RPE interface are the site of the earliest central retinal abnormalities detectable clinically in CHM (Fig. 5D).

DISCUSSION

A large body of literature on the disease expression of CHM hemizygotes has accumulated from its original description over a century ago. Most studies have focused on changes in VA and/or peripheral visual field extent measured by kinetic perimetry, with a minority addressing disease progression quantitatively with data from psychophysics, detailed retinal imaging or electrophysiology, a handful longitudinally, most retrospectively.[1-14,49-73] A detailed cross-sectional evaluation of the retinal structure in large groups of patients with this disease at various stages constitutes a practical alternative to partially overcome the relative lack of longitudinal information imposed by this slowly progressive, infrequent disease. This study, which took place in preparation for a gene therapy trial for CHM to be conducted at the University of Pennsylvania prospectively evaluated one of the largest samples of CHM patients characterized quantitatively with SD-OCT to date.

We confirmed degenerative changes and visual dysfunction in the central retina at the earliest ages sampled, which progressed in a centripetal fashion following the steps of a model of disease progression proposed a decade ago and consistent with previous reports in young patients.[7,8,10,51] There was a suggestion of a fast decline in the extent of relative EZ and RPE preservation in patients younger than 20 years of age, consistent with previous observations.[11] However, steep transitions in retinal structure, which delimit relatively preserved from degenerated central retina, moved centripetally from the pericentral retina at a very slow rate of (~0.3° per year) for ages >20 years. We found that the disease expression was quite symmetric for patients younger than 30 years of age but that there was a tendency for an increase in IOD variability in all parameters examined with increasing age, although the differences between different age subgroups did not reach statistical significance ($P>0.05$)(Table 2). The findings raise important questions regarding patient inclusion criteria for participation in clinical trials as well as for the selection of outcome measures. The slow progression of the central degeneration in CHM will constitute a challenge for the interpretation of outcomes for gene augmentation trials aimed at treating residual central islands of cones that are relatively resistant to degeneration as longer observation times may be required to assess treatment outcomes. The main rates of progression estimated from our large cross-sectional data represented an interval nearly equivalent to a human life-span and used parameters measured manually after visual confirmation of the disappearance of the ONL and EZ layers and corresponding signal features on LRPs. Establishing the significance of short-term structural change in CHM will benefit from the development of automatic measures of the lateral extent of the structural parameters and the study of the

short-term inter-visit and inter-observer (or inter-algorithm) variability of the measurements in longitudinal studies, which fell outside the scope of the present work and limits the applicability of our observations to finer changes and observation intervalsLongitudinal observation of individual patients with the use of refined, more sensitive outcome measures is needed to provide short-term measures of safety and efficacy.

The relative long ‘life expectancy’ of high level of central function resulting from the slow rates of progression in CHM poses additional risk:benefit dilemmas if the presumably fast progressing extrafoveal/midperipheral retina is alternatively targeted in interventional studies. Such interventions will expose the neighboring central region, critical for the patients’ quality of life, to the risks of an invasive subretinal surgery. A decision to enroll younger individuals should be made knowing that it may not be safe to re-administer a treatment to the central retina of that same eye at a later age due to the potential for an immune response.

Variability in disease expression, including well-documented intrafamilial variability in this otherwise molecularly homogenous disease, suggests that historical data, both cross-sectional and longitudinal, although important for patient counseling, will be of limited use to serve as universal templates against which safety and/or efficacy of treatments may be evaluated. Intraretinal comparisons between treated and untreated retina widely exploited in the *RPE65*-LCA trials may not be possible in CHM or other inherited retinal diseases at stages where small residual small islands of treatable tissue are all that is left. Interocular comparisons of various structural and functional parameters may be used instead as an alternative. Selection of older patients and/or later disease stages, however, may limit the use of interocular comparisons as the disease may become more asymmetric and less predictable as suggested by our study and previous reports.[10,13] Careful consideration of each of the factors discussed above will have to take place during the preparation and enrollment phases of the growing number of clinical trials planned for CHM.

Central retinal abnormalities were observed in all our young patients (age ≤15 years), including the youngest, at age 6. The earliest abnormality was the approximation of the EZ to the RPE and/or loss of the IZ signal, likely representing shortening or loss of the POS. These abnormalities were observed in areas with normal appearing RPE pigmentation, and also coincided with ONL preservation in most individuals. POS abnormalities documented by histology in a young patient with CHM appear to precede retinal remodeling as the first stage in a model of CHM.[8,74] The EZ-to-RPE distance, which includes the length of the POS, measured in a large number of locations (n=14196) with preserved EZ and RPE melanin confirmed this qualitative observation. There were no examples of areas of depigmentation with normal overlying POS. Although the primary site of disease in CHM remains debatable with later trends pointing toward the RPE, our findings are consistent with a rod POS abnormality resulting in rod dysfunction as the earliest detectable abnormality within the central retina in CHM, consistent with previous observations and with reports of impaired night vision, early rod dysfunction and histological evidence of rod disease in CHM.[7,8,51,70,75,76] Although our findings point strongly at rod photoreceptors as the primary site of insult as a result of the loss of *REP1* function the possibility still exists that rods may be particularly vulnerable to a primary RPE abnormality that takes place

before obvious RPE disease becomes clinically detectable as demelanization. Evidence for early (and late) cone photoreceptor disease has accumulated for over four decades and was corroborated in this cohort.[7,8,10,50,51,66,70,] Measurable ONL in blind regions of severe RPE demelanization and choroidal thinning suggests survival of photoreceptors, likely cones, in severe RPE and choroidal disease. This indeed departs from the sequence of primary rod photoreceptor disease where RPE demelanization and choroidal abnormalities tend to occur following total photoreceptor loss.[77,78] Cone photoreceptor survival in the presence of severe RPE disease supports a relative resistance of cones to a preceding, parallel or relatively independent RPE abnormality.[50,79-81] Detectable ONL, at times, several millimeters peripheral to central regions of relative RPE and POS preservation may constitute a '*penumbra zone*' of surviving photoreceptors that may be able to regain some degree of functionality following efficacious therapeutic interventions. Measuring residual vision in such regions, including in TZs, poses a significant challenge.[33,43] End-stage disease showed relative preservation of the inner retina in regions with otherwise severe outer retina/RPE/choroidal disease, consistent with earlier histopatologic reports.[76,82-84] Treatment alternatives that require a viable inner retina when the outer retina and/or the RPE are no longer available for gene augmentation may still be possible for such patients.[85-87]

The sequence of central disease progression generated from this cross-sectional data confirmed and expanded on a disease model proposed by Jacobson et al.[8] In that model initial retinal thickening as a consequence of retinal remodeling precedes retinal thinning and cone sensitivity loss.[7,8,10] Relative preservation of residual central islands supporting VA better than 20/40, even in end-stage disease has long been recognized in CHM.[4,6-12] Rates of VA change (~0.05 logMAR/year) following decades of relative stability in this cohort are comparable to previous reports.[6,10-12] Foveal sensitivity loss with increasing age found in a subgroup of our patients is likely the consequence of COS abnormalities and/or cone loss which has been documented in early CHM, before severe abnormalities of RPE pigmentation reach the foveal center.[7,8] There was an indication that the rate of decline (~0.5-2dB/year) may be greater after the fourth decade of life. VA preservation despite progressive structural and functional loss makes VA a poor measure of central disease severity as well as a suboptimal outcome measure for CHM clinical trials, except for particular stages of the disease or as a measure of safety.[33,34] We found that VA correlated with total foveal (or foveal ONL) thickness. The slope of the relationship was steeper in older ages when associated abnormalities, such as the presence of intraretinal bridges or EZ/POS disruptions, take place as the TZ approximates the foveal center. However, we also found foveal abnormalities that occurred in young patients before close approximation of the TZs to the fovea and which may similarly indicate an impending decline in foveal function.[8] The sequence of events that lead to early macular hole formation and central retinoschisis in CHM are not fully understood, but may be a consequence of a remodeling response to photoreceptor degeneration.[8,46-48] The findings dictate caution when considering inclusion of patients in gene therapy trials involving subretinal injections when such foveal abnormalities are observed, particularly in patients with abnormally thin retinas or when TZ boundaries are seen in close proximity (<500 μm) of the foveal center. If such patients are included, then to limit mechanical trauma to fragile photoreceptors it may be advisable to place retinotomies as far from the foveal center as possible (while in non-atrophic retina),

limit the total volume of the subretinal injections to the minimum needed to achieve coverage of the residual islands of preserved photoreceptors/RPE, while ensuring that the subretinal bleb boundaries extend beyond the foveal center (i.e. not bisecting the fovea/parafovea).

Ongoing phase I/II gene therapy trials for CHM have included patients at later stages of the disease with only residual central islands of relatively preserved retina, the only available target for such intervention at that stage of the disease. Better understanding of the natural history of the central structural changes in CHM and their relationship with vision will help establish patients' candidacy for inclusion in such trials as well as the adoption of appropriate outcome measures with which to assess the safety and efficacy of this intervention. Regional differences in the horizontal extent of relatively preserved central retina and/or vision in CHM measured in this study and documented by others suggest intraretinal variation in disease severity and progression rates.[4,8,13,43,50,65] Of interest, a similar pattern of disease predilection for the nasal pericentral and peripapillary retina was reported in Bietti crystalline dystrophy, a disease that shares with CHM the presence of regions of scalloped central chorioretinal atrophy.[40] Further characterization of the extramacular retina at earlier disease stages in CHM, which was not addressed in our study, is also needed to better define possible regional differences in disease expression that may be exploited to shorten the length of observation intervals required to unambiguously detect progression. The quantitative measures of the central retinal structure used in this study painted a picture of the natural history of CHM over the age span of over seven decades that may serve as a reference for the design of clinical trials testing therapeutic approaches.

Supplementary Material

Refer to Web version on PubMed Central for supplementary material.

Acknowledgements

Thanks are due to Elena M. Aleman, Katherine E. Uyhazi and Elaine J. Zhou for their critical help.

Supported by grants from the National Institutes of Health (NEI-K12EY015398-10, U01EY025477,P30EY01583-26), Hope for Vision, The Foundation Fighting Blindness, The Choroideremia Research Foundation, Macula Vision Research Foundation, The Paul and Evanina Bell Mackall Foundation Trust, The Pennsylvania Lions Sight Conservation and Research Foundation and Research to Prevent Blindness.

REFERENCES

1. Kurstjens JH. Choroideremia and gyrate atrophy of the choroid and retina. Doc Ophthalmol. 1965; 19:1–122.
2. McCulloch C. Choroideremia: a clinical and pathologic review. Trans Am Ophthalmol Soc. 1969; 67:142–195. [PubMed: 5381297]
3. MacDonald, IM., Hume, S., Chan, S., Seabra, MC., Pagon, RA., Adam, MP., Ardinger, HH., Wallace, SE., Amemiya, A., Bean, LJH., Bird, TD., Ledbetter, N., Mefford, HC., Smith, RJH., Stephens, K. GeneReviews® [Internet]. University of Washington, Seattle; Seattle (WA): 1993-2016. Choroideremia. Available from: http://www.ncbi.nlm.nih.gov/books/NBK1337/
4. Kärnä J, Choroideremia. A clinical and genetic study of 84 Finnish patients and 126 female carriers. Acta Ophthalmol Suppl. 1986; 176:1–68. [PubMed: 3014804]

5. McCulloch C, McCulloch RJ. A hereditary and clinical study of choroideremia. Trans Am Acad Ophthalmol Otolaryngol. 1948; 52:160–190. [PubMed: 18901798]
6. Hayakawa M, Fujiki K, Hotta Y, Ito R, Ohki J, Ono J, Saito A, Nakayasu K, Kanai A, Ishidoh K, Kominami E, Yoshida K, Kim KC, Ohashi H. Visual impairment and *REP-1* gene mutations in Japanese choroideremia patients. Ophthalmic Genet. 1999; 20:107–115. [PubMed: 10420196]
7. Duncan JL, Aleman TS, Gardner LM, De Castro E, Marks DA, Emmons JM, Bieber ML, Steinberg JD, Bennett J, Stone EM, MacDonald IM, Cideciyan AV, Maguire MG, Jacobson SG. Macular pigment and lutein supplementation in choroideremia. Exp Eye Res. 2002; 74:371–81. [PubMed: 12014918]
8. Jacobson SG, Cideciyan AV, Sumaroka A, Aleman TS, Schwartz SB, Windsor EA, Roman AJ, Stone EM, MacDonald IM. Remodeling of the human retina in choroideremia: rab escort protein 1 (*REP-1*) mutations. Invest Ophthalmol Vis Sci. 2006; 47:4113–4120. [PubMed: 16936131]
9. Roberts MF, Fishman GA, Roberts DK, Heckenlively JR, Weleber RG, Anderson RJ, Grover S. Retrospective, longitudinal, and cross sectional study of visual acuity impairment in choroideraemia. Br J Ophthalmol. 2002; 86:658–62. [PubMed: 12034689]
10. Heon E, Alabduljalil T, Iii DB, Cideciyan AV, Li S, Chen S, Jacobson SG. Visual function and central retinal structure in choroideremia. Invest Ophthalmol Vis Sci. 2016; 57:OCT377–OCT387. [PubMed: 27409497]
11. Nabholz N, Lorenzini MC, Bocquet B, Lacroux A, Faugère V, Roux AF, Kalatzis V, Meunier I, Hamel CP. Clinical evaluation and cone alterations in choroideremia. Ophthalmology. 2016; 123:1830–1832. [PubMed: 26992839]
12. Coussa RG, Traboulsi EI. Choroideremia: a review of general findings and pathogenesis. Ophthalmic Genet. 2012; 33:57–65. [PubMed: 22017263]
13. Seitz IP, Zhour A, Kohl S, Llavona P, Peter T, Wilhelm B, Zrenner E, Ueffing M, Bartz-Schmidt KU, Fischer MD. Multimodal assessment of choroideremia patients defines pre-treatment characteristics. Graefes Arch Clin Exp Ophthalmol. 2015; 253:2143–2150. [PubMed: 25744334]
14. Pameyer JK, Waardenburg PJ, Henkes HE. Choroideremia. Br. J. Ophthalmol. 1960; 44:724–738. [PubMed: 13732369]
15. Cremers FP, van de Pol DJ, van Kerkhoff LP, Wieringa B, Ropers HH. Cloning of a gene that is rearranged in patients with choroideraemia. Nature. 1990; 347:674–677. [PubMed: 2215697]
16. Merry DE, Jänne PA, Landers JE, Lewis RA, Nussbaum RL. Isolation of a candidate gene for choroideremia. Proc Natl Acad Sci U S A. 1992; 89:2135–2139. [PubMed: 1549574]
17. Sankila EM, Tolvanen R, van den Hurk JA, Cremers FP, de la Chapelle A. Aberrant splicing of the CHM gene is a significant cause of choroideremia. Nat Genet. 1992; 1:109–113. [PubMed: 1302003]
18. van Bokhoven H, Schwartz M, Andréasson S, van den Hurk JA, Bogerd L, Jay M, Rüther K, Jay B, Pawlowitzki IH, Sankila EM, et al. Mutation spectrum in the CHM gene of Danish and Swedish choroideremia patients. Hum Mol Genet. 1994; 3:1047–1051. [PubMed: 7981671]
19. van den Hurk JA, Schwartz M, van Bokhoven H, van de Pol TJ, Bogerd L, Pinckers AJ, Bleeker-Wagemakers EM, Pawlowitzki IH, Rüther K, Ropers HH, Cremers FP. Molecular basis of choroideremia (CHM): mutations involving the Rab escort protein-1 (*REP-1*) gene. Hum Mutat. 1997; 9:110–117. [PubMed: 9067750]
20. Seabra MC, Brown MS, Goldstein JL. Retinal degeneration in choroideremia: deficiency of rab geranylgeranyl transferase. Science. 1993; 259:377–381. [PubMed: 8380507]
21. Seabra MC, Mules EH, Hume AN. Rab GTPases, intracellular traffic and disease. Trends Mol Med. 2002; 8:23–30. [PubMed: 11796263]
22. MacDonald IM, Mah DY, Ho YK, Lewis RA, Seabra MC. A practical diagnostic test for choroideremia. Ophthalmology. 1998; 105:1637–1640. [PubMed: 9754170]
23. MacDonald IM, Sereda C, McTaggart K, Mah D. Choroideremia gene testing. Expert Rev Mol Diagn. 2004; 4:478–484. [PubMed: 15225095]
24. Seabra MC, Ho YK, Anant JS. Deficient geranylgeranylation of Ram/Rab27 in choroideremia. J Biol Chem. 1995; 270:24420–24427. [PubMed: 7592656]
25. Preising M, Ayuso C. Rab escort protein 1 (*REP1*) in intracellular traffic: a functional and pathophysiological overview. Ophthalmic Genet. 2004; 25:101–110. [PubMed: 15370541]

26. Sergeev YV, Smaoui N, Sui R, Stiles D, Gordiyenko N, Strunnikova N, Macdonald IM. The functional effect of pathogenic mutations in Rab escort protein 1. Mutat Res. 2009; 665:44–50. [PubMed: 19427510]
27. Dimopoulos IS, Chan S, MacLaren RE, MacDonald IM. Pathogenic mechanisms and the prospect of gene therapy for choroideremia. Expert Opin Orphan Drugs. 2015; 3:787–798. [PubMed: 26251765]
28. Zhang AY, Mysore N, Vali H, Koenekoop J, Cao SN, Li S, Ren H, Keser V, Lopez-Solache I, Siddiqui SN, Khan A, Mui J, Sears K, Dixon J, Schwartzentruber J, Majewski J, Braverman N, Koenekoop RK. Choroideremia is a systemic disease with lymphocyte crystals and plasma lipid and RBC membrane abnormalities. Invest Ophthalmol Vis Sci. 2015; 56:8158–8165. [PubMed: 26720468]
29. Jacobson SG, Cideciyan AV, Aguirre GD, Roman AJ, Sumaroka A, Hauswirth WW, Palczewski K. Improvement in vision: a new goal for treatment of hereditary retinal degenerations. Expert Opin Orphan Drugs. 2015; 3:563–575. [PubMed: 26246977]
30. Jacobson SG, Cideciyan AV, Roman AJ, Sumaroka A, Schwartz SB, Heon E, Hauswirth WW. Improvement and decline in vision with gene therapy in childhood blindness. New Engl J Med. 2015; 372:1920–1926. [PubMed: 25936984]
31. Bennett J, Wellman J, Marshall KA, McCague S, Ashtari M, DiStefano-Pappas J, Elci OU, Chung DC, Sun J, Wright JF, Cross DR, Aravand P, Cyckowski LL, Bennicelli JL, Mingozzi F, Auricchio A, Pierce EA, Ruggiero J, Leroy BP, Simonelli F, High KA, Maguire AM. Safety and durability of effect of contralateral-eye administration of AAV2 gene therapy in patients with childhood-onset blindness caused by *RPE65* mutations: a follow-on phase 1 trial. Lancet. Jun 30.2016 pii: S0140-6736(16)30371-3.
32. Pierce EA, Bennett J. The status of *RPE65* gene therapy trials: safety and efficacy. Cold Spring Harb Perspect Med. 2015; 5:a017285. [PubMed: 25635059]
33. MacLaren RE, Groppe M, Barnard AR, Cottriall CL, Tolmachova T, Seymour L, Clark KR, During MJ, Cremers FP, Black GC, Lotery AJ, Downes SM, Webster AR, Seabra MC. Retinal gene therapy in patients with choroideremia: initial findings from a phase 1/2 clinical trial. Lancet. 2014; 383:1129–1137. [PubMed: 24439297]
34. Edwards TL, Jolly JK, Groppe M, Barnard AR, Cottriall CL, Tolmachova T, Black GC, Webster AR, Lotery AJ, Holder GE, Xue K, Downes SM, Simunovic MP, Seabra MC, MacLaren RE. Visual acuity after retinal gene therapy for choroideremia. N Engl J Med. 2016; 374:1996–1998. [PubMed: 27120491]
35. Chan SC, Bubela T, Dimopoulos IS, Freund PR, Varkouhi AK, MacDonald IM. Choroideremia research: report and perspectives on the second international scientific symposium for choroideremia. Ophthalmic Genet. 2016; 8:1–9.
36. Huckfeldt RM, Bennett J. Promising first steps in gene therapy for choroideremia. Hum Gene Ther. 2014; 25:96–97. [PubMed: 24502407]
37. Curcio CA, Messinger JD, Sloan KR, Mitra A, McGwin G, Spaide RF. Human chorioretinal layer thicknesses measured in macula-wide, high-resolution histologic sections. Invest Ophthalmol Vis Sci. 2011; 52:3943–3954. [PubMed: 21421869]
38. Jacobson SG, Voigt WJ, Parel JM, Apáthy PP, Nghiem-Phu L, Myers SW, Patella VM. Automated light- and dark-adapted perimetry for evaluating retinitis pigmentosa. Ophthalmology. 1986; 93:1604–1611. [PubMed: 3808619]
39. Aleman TS, Cideciyan AV, Sumaroka A, Windsor EAM, Herrera W, White DA, Kaushal S, Naidu A, Roman AJ, Schwartz SB, Stone EM, Jacobson SG. Retinal laminar architecture in human retinitis pigmentosa caused by *rhodopsin* gene mutations. Invest. Ophthalmol. Vis. Sci. 2008; 49:1580–1590. [PubMed: 18385078]
40. Fuerst NM, Serrano L, Han G, Morgan JIW, Maguire AMM, Leroy BP, Kim BJ, Aleman TS. Detailed functional and structural phenotype of Bietti crystalline dystrophy associated with mutations in *CYP4V2* complicated by choroidal neovascularization. Ophthalmic Genetics. 2016; 30:1–8.
41. Liang KY, Zeger SL. Longitudinal data analysis using generalized linear models. Biometrika. 1986; 73:13–22.

42. Cideciyan AV, Swider M, Jacobson SG. Autofluorescence imaging with near-infrared excitation: normalization by reflectance to reduce signal from choroidal fluorophores. Invest Ophthalmol Vis Sci. 2015; 56:3393–3406. [PubMed: 26024124]
43. Lazow MA, Hood DC, Ramachandran R, Burke TR, Wang YZ, Greenstein VC, Birch DG. Transition zones between healthy and diseased retina in choroideremia (CHM) and Stargardt disease (STGD) as compared to retinitis pigmentosa (RP). Invest Ophthalmol Vis Sci. 2011; 52:9581–9590. [PubMed: 22076985]
44. Xue K, Oldani M, Jolly JK, Edwards TL, Groppe M, Downes SM, MacLaren RE. Correlation of optical coherence tomography and autofluorescence in the outer retina and choroid of patients with choroideremia. Invest Ophthalmol Vis Sci. 2016; 57:3674–3684. [PubMed: 27403996]
45. Aleman TS, Cideciyan AV, Sumaroka A, Schwartz SB, Roman AJ, Windsor EAM, Steinberg JD, Branham K, Othman M, Swaroop A, Jacobson SG. Inner retinal abnormalities in X-linked retinitis pigmentosa with RPGR mutations. Invest. Ophthalmol. Vis. Sci. 2007; 48:4759–4765. [PubMed: 17898302]
46. Cour M, Friis J. Macular holes: classification, epidemiology, natural history and treatment. Acta Ophthalmol. Scand. 2002; 80:579–587. [PubMed: 12485276]
47. Zinkernagel MS, Groppe M, MacLaren RE. Macular hole surgery in patients with end-stage choroideremia. Ophthalmology. 2013; 120:1592–1596. [PubMed: 23562166]
48. Shinoda H, Koto T, Fujiki K, Murakami A, Tsubota K, Ozawa Y. Clinical findings in a choroideremia patient who underwent vitrectomy for retinal detachment associated with macular hole. Jpn J Ophthalmol. 2011; 55:169–171. [PubMed: 21400066]
49. Sorsby A, Franceschetti A, Joseph R, Davey JB. Choroideremia; clinical and genetic aspects. Br J Ophthalmol. 1952; 36:547–581. [PubMed: 12978235]
50. Syed R, Sundquist SM, Ratnam K, Zayit-Soudry S, Zhang Y, Crawford JB, MacDonald IM, Godara P, Rha J, Carroll J, Roorda A, Stepien KE, Duncan JL. High-resolution images of retinal structure in patients with choroideremia. Invest Ophthalmol Vis Sci. 2013; 54:950–961. [PubMed: 23299470]
51. Morgan JI, Han G, Klinman E, Maguire WM, Chung DC, Maguire AM, Bennett J. High-resolution adaptive optics retinal imaging of cellular structure in choroideremia. Invest Ophthalmol Vis Sci. 2014; 55:6381–6397. [PubMed: 25190651]
52. Katz BJ, Yang Z, Payne M, Lin Y, Zhao Y, Pearson E, Duan S, Kamaya S, Karan G, Zhang K. Fundus appearance of choroideremia using optical coherence tomography. Adv Exp Med Biol. 2006; 572:57–61. [PubMed: 17249555]
53. Jia Y, Bailey ST, Hwang TS, McClintic SM, Gao SS, Pennesi ME, Flaxel CJ, Lauer AK, Wilson DJ, Hornegger J, Fujimoto JG, Huang D. Quantitative optical coherence tomography angiography of vascular abnormalities in the living human eye. Proc Natl Acad Sci U S A. 2015; 112:E2395–2402. [PubMed: 25897021]
54. Genead MA, McAnany JJ, Fishman GA. Retinal nerve fiber thickness measurements in choroideremia patients with spectral-domain optical coherence tomography. Ophthalmic Genet. 2011; 32:101–106. [PubMed: 21268676]
55. Genead MA, Fishman GA. Cystic macular oedema on spectral-domain optical coherence tomography in choroideremia patients without cystic changes on fundus examination. Eye (Lond). 2011; 25:84–90. [PubMed: 20966974]
56. Francis PJ, Fishman GA, Trzupek KM, MacDonald IM, Stone EM, Weleber RG. Stop mutations in exon 6 of the choroideremia gene, CHM, associated with preservation of the electroretinogram. Arch Ophthalmol. 2005; 123:1146–1149. [PubMed: 16087855]
57. Garcia-Hoyos M, Lorda-Sanchez I, Gómez-Garre P, Villaverde C, Cantalapiedra D, Bustamante A, Diego-Alvarez D, Vallespin E, Gallego-Merlo J, Trujillo MJ, Ramos C, Ayuso C. New type of mutations in three spanish families with choroideremia. Invest Ophthalmol Vis Sci. 2008; 49:1315–1321. [PubMed: 18385043]
58. Huang AS, Kim LA, Fawzi AA. Clinical characteristics of a large choroideremia pedigree carrying a novel CHM mutation. Arch Ophthalmol. 2012; 130:1184–9. [PubMed: 22965595]

59. Mura M, Sereda C, Jablonski MM, MacDonald IM, Iannaccone A. Clinical and functional findings in choroideremia due to complete deletion of the *CHM* gene. Arch Ophthalmol. 2007; 125:1107–1113. [PubMed: 17698759]
60. Coussa RG, Kim J, Traboulsi EI. Choroideremia: effect of age on visual acuity in patients and female carriers. Ophthalmic Genet. 2012; 33:66–73. [PubMed: 22060191]
61. Esposito G, De Falco F, Tinto N, Testa F, Vitagliano L, Tandurella IC, Iannone L, Rossi S, Rinaldi E, Simonelli F, Zagari A, Salvatore F. Comprehensive mutation analysis (20 families) of the choroideremia gene reveals a missense variant that prevents the binding of REP1 with Rab geranylgeranyl transferase. Hum Mutat. 2011; 32:1460–1469. [PubMed: 21905166]
62. Grover S, Alexander KR, Fishman GA, Ryan J. Comparison of intraocular light scatter in carriers of choroideremia and X-linked retinitis pigmentosa. Ophthalmology. 2002; 109:159–163. [PubMed: 11772598]
63. Grover S, Alexander KR, Choi DM, Fishman GA. Intraocular light scatter in patients with choroideremia. Ophthalmology. 1998; 105:1641–1645. [PubMed: 9754171]
64. Iino Y, Fujimaki T, Fujiki K, Murakami A. A novel mutation (967-970+2)delAAAGGT in the choroideremia gene found in a Japanese family and related clinical findings. Jpn J Ophthalmol. 2008; 52:289–297. [PubMed: 18773267]
65. Jain N, Jia Y, Gao SS, Zhang X, Weleber RG, Huang D, Pennesi ME. Optical coherence tomography angiography in choroideremia: correlating choriocapillaris loss with overlying degeneration. JAMA Ophthalmol. 2016; 134:697–702. [PubMed: 27149258]
66. Jolly JK, Groppe M, Birks J, Downes SM, MacLaren RE. Functional Defects in Color Vision in Patients With Choroideremia. Am J Ophthalmol. 2015; 160:822–831. [PubMed: 26133251]
67. Lin Y, Liu X, Luo L, Qu B, Jiang S, Yang H, Liang X, Ye S, Liu Y. Molecular analysis of the choroideremia gene related clinical findings in two families with choroideremia. Mol Vis. 2011; 17:2564–2569. [PubMed: 22025891]
68. Ponjavic V, Abrahamson M, Andréasson S, Van Bokhoven H, Cremers FP, Ehinger B, Fex G. Phenotype variations within a choroideremia family lacking the entire CHM gene. Ophthalmic Genet. 1995; 16:143–150. [PubMed: 8749050]
69. Renner AB, Kellner U, Cropp E, Preising MN, MacDonald IM, van den Hurk JA, Cremers FP, Foerster MH. Choroideremia: variability of clinical and electrophysiological characteristics and first report of a negative electroretinogram. Ophthalmology. 2006; 113:2066, e1–10. [PubMed: 16935340]
70. Rubin ML, Fishman RS, McKay RA. Choroideremia. Study of a family and literature review. Arch Ophthalmol. 1966; 76:563–574. [PubMed: 5928144]
71. Sanchez-Alcudia R, Garcia-Hoyos M, Lopez-Martinez MA, Sanchez-Bolivar N, Zurita O, Gimenez A, Villaverde C, Rodrigues-Jacy da Silva L, Corton M, Perez-Carro R, Torriano S, Kalatzis V, Rivolta C, Avila-Fernandez A, Lorda I, Trujillo-Tiebas MJ, Garcia-Sandoval B, Lopez-Molina MI, Blanco-Kelly F, Riveiro-Alvarez R, Ayuso C. A comprehensive analysis of Choroideremia: From genetic characterization to clinical practice. PLoS One. 2016; 11:e0151943. [PubMed: 27070432]
72. Sieving PA, Niffenegger JH, Berson EL. Electroretinographic findings in selected pedigrees with choroideremia. Am J Ophthalmol. 1986; 101:361–367. [PubMed: 3953730]
73. Lee TK, McTaggart KE, Sieving PA, Heckenlively JR, Levin AV, Greenberg J, Weleber RG, Tong PY, Anhalt EF, Powell BR, MacDonald IM. Clinical diagnoses that overlap with choroideremia. Can J Ophthalmol. 2003; 38:364–372. [PubMed: 12956277]
74. Rodrigues MM, Ballintine EJ, Wiggert BN, Lee L, Fletcher RT, Chader GJ. Choroideremia: a clinical, electron microscopic, and biochemical report. Ophthalmology. 1984; 91:873–883. [PubMed: 6089068]
75. Syed N, Smith JE, John SK, Seabra MC, Aguirre GD, Milam AH. Evaluation of retinal photoreceptors and pigment epithelium in a female carrier of choroideremia. Ophthalmology. 2001; 108:711–720. [PubMed: 11297488]
76. MacDonald IM, Russell L, Chan CC. Choroideremia: new findings from ocular pathology and review of recent literature. Surv Ophthalmol. 2009; 54:401–407. [PubMed: 19422966]

77. Wright AF, Chakarova CF, Abd El-Aziz MM, Bhattacharya SS. Photoreceptor degeneration: genetic and mechanistic dissection of a complex trait. Nat Rev Genet. 2010; 11:273–284. [PubMed: 20212494]

78. Milam AH, Li ZY, Fariss RN. Histopathology of the human retina in retinitis pigmentosa. Prog Retin Eye Res. 1998; 17:175–205. [PubMed: 9695792]

79. Tolmachova T, Anders R, Abrink M, et al. Independent degeneration of photoreceptors and retinal pigment epithelium in conditional knockout mouse models of choroideremia. J Clin Invest. 2006; 116:386–394. [PubMed: 16410831]

80. Tolmachova T, Wavre-Shapton ST, Barnard AR, MacLaren RE, Futter CE, Seabra MC. Retinal pigment epithelium defects accelerate photoreceptor degeneration in cell type-specific knockout mouse models of choroideremia. Invest Ophthalmol Vis Sci. 2010; 51:4913–4920. [PubMed: 20445111]

81. Hawkins RK, Jansen HG, Sanyal S. Development and degeneration of retina in rds mutant mice: photoreceptor abnormalities in the heterozygotes. Exp Eye Res. 1985; 41:701–720. [PubMed: 3830736]

82. Ghosh M, McCulloch JC. Pathological findings from two cases of choroideremia. Can J Ophthalmol. 1980; 15:147–153. [PubMed: 6969107]

83. Rafuse EV, McCulloch C. Choroideremia. A pathological report. Can J Ophthalmol. 1968; 3:347–352. [PubMed: 5727760]

84. McCulloch C, McCulloch RJ. Choroideremia; a hereditary and clinical study. Arch Ophthal. 1950; 43:179–181.

85. Jacobson SG, Matsui R, Sumaroka A, Cideciyan AV. Retinal structure measurements as inclusion criteria for stem cell-based therapies of retinal degenerations. Invest Ophthalmol Vis Sci. 2016; 57 ORSFn1-9.

86. Duebel J, Marazova K, Sahel JA. Optogenetics. Curr Opin Ophthalmol. 2015; 26:226–232. [PubMed: 25759964]

87. Yue L, Weiland JD, Roska B, Humayun MS. Retinal stimulation strategies to restore vision: Fundamentals and systems. Prog Retin Eye Res. 2016; 53:21–47. [PubMed: 27238218]

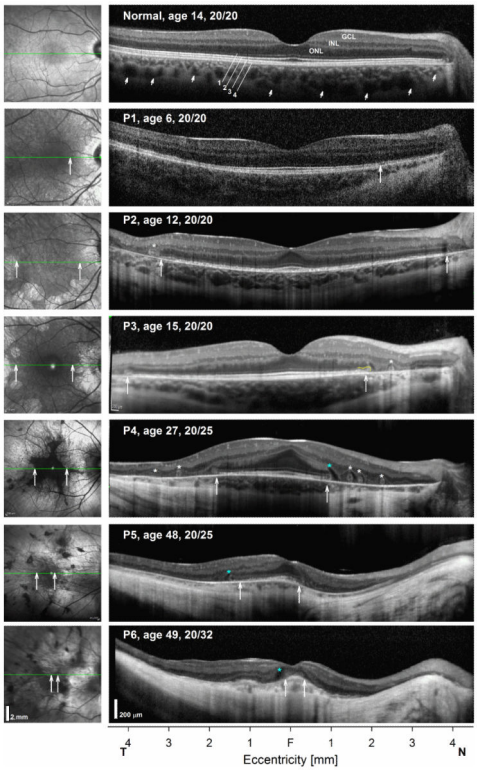

FIGURE 1.

Progression of central structural changes in CHM. Shown are 9 mm-long horizontal SD-OCT cross-sections (right panels) through the fovea in a normal subject compared with five CHM patients representing different disease stages. Nuclear layers are labeled on the normal subject; outer photoreceptor/RPE laminae are numbered (1, ELM; 2, EZ; 3 IZ; 4, RPE), following conventional terminology. Patient's ages and VA at time of examination are shown. NIR-REF images are shown to the left of the SD-OCT cross sections; green lines superimposed on the images indicate the location of the scan. All eyes are shown as right eyes scanning following a temporal to nasal direction. Asterisks positioned near the OPL denote locations with outer retinal tubulations (*white asterisks*) or with intraretinal hyperreflectivities (*blue*). Vertical arrows demarcate lateral extent of uninterrupted EZ at the edge of TZs. The distal outward evagination of the ELM at the nasal TZ of P2 is highlighted in yellow.

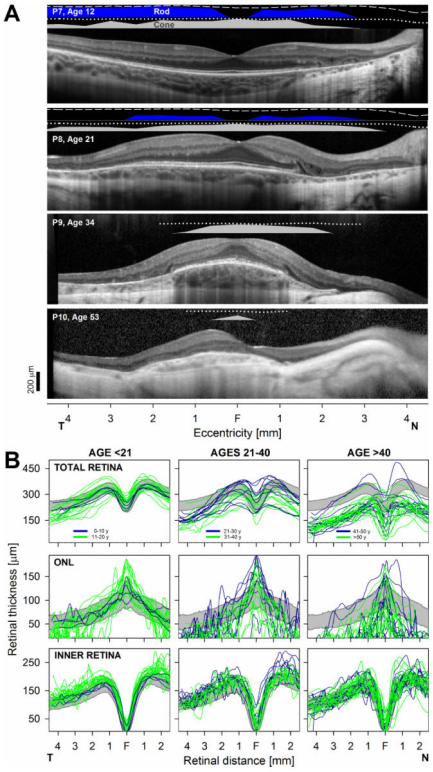

FIGURE 2.

Structure and function correlations in CHM. **A.** 9 mm-long, non-straightened, SD-OCT cross-sections along the horizontal meridian through the fovea in patients with the earliest central abnormalities (*top two panels*) are compared with patients (bottom two panels) with the later abnormalities. Nuclear layers are labeled in Fig 1. Bars above the scans show psychophysically determined rod (*blue bar*: dark-adapted, 500-nm stimulus) and cone (*gray bar*: light-adapted, white stimulus) sensitivities. Lines above bars define lower limit (mean-2SD) of sensitivity for the dark-adapted (*dashed lines*) and light-adapted (*dotted lines*) conditions in normal subjects. T, temporal retina; N, nasal retina. Calibration bar to the bottom left. **B.** Overall retinal (total), inner retinal and ONL thicknesses along the horizontal meridian from all patients grouped by age segments roughly representing early (*left panels*), intermediate (*middle panels*) and late stages (right panels) of the disease. Within each age segment measurements are further subdivided into a first decade (*blue traces*) and second decade (*green traces*). Gray bands: normal limits (mean ± 2SD; $n = 44$, age range, 11-49). Only one eye shown for clarity.

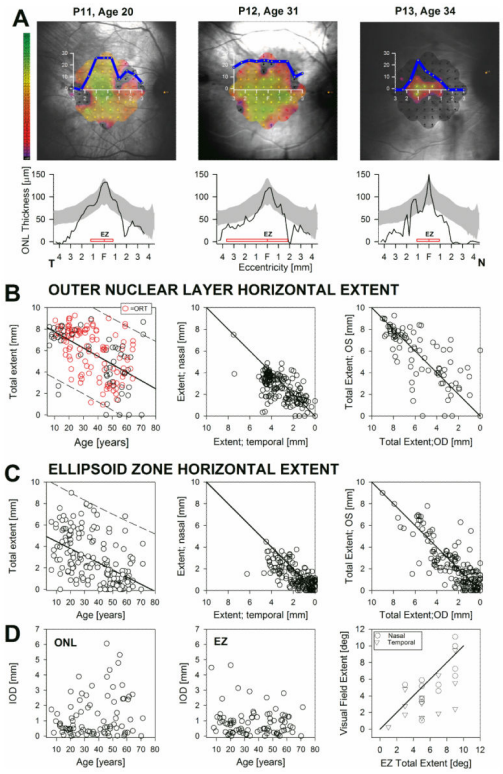

FIGURE 3.

Spatial progression of the central structural and functional changes in CHM. **A.** *Top panels:* sensitivity values determined with microperimetry using a 10-2 protocol (dark-adapted) and a 0.45°diameter white stimuli in representativ e patients with limited extents of viable central retina and steady foveal fixation. Sensitivity values are coded to a pseudocolor scale (left; 0 to 36 dB; mean normal = 30 dB = mid-range green) and shown overlaid an IR-REF image of the fundus obtained during the test. Superimposed is an average horizontal sensitivity profile (blue line) obtained by averaging sensitivities for locations above and below (±1°) the horizontal meridian of the 10-2 protocol grid. *Bottom panels:* ONL thickness plotted as a function of eccentricity for the patients shown in top panels. Gray bands: normal limits (mean ± 2SD; n = 44, age range, 11-49). Horizontal red bars: lateral extent of uninterrupted the EZ. **B,C** Total horizontal extent (temporal+nasal) of the ONL (**B**) and EZ (**C**) layers plotted as a function of age (*left panels*), as plots of the nasal versus the temporal extent (*middle panel*) of the right eye plotted against the contralateral eye (*right panels*) extent for both retinal layers. Solid lines are the linear regression fit to the data with 95% prediction intervals (*dashed lines*) (*left panels*) or equality lines (center and right). (**D**) Intraocular differences (IOD) for ONL and EZ total horizontal extent plotted as a function of age (*left and center*) and microperimetric visual field extent (*right panel*) as analyzed in (A) from both eyes of a subset of patients (n = 16) with CHM plotted against EZ horizontal extent. Solid line is a linear regression fit to the data. EZ extent is expressed in degrees for ease of comparison with data in 10-2 protocol grid of (A).

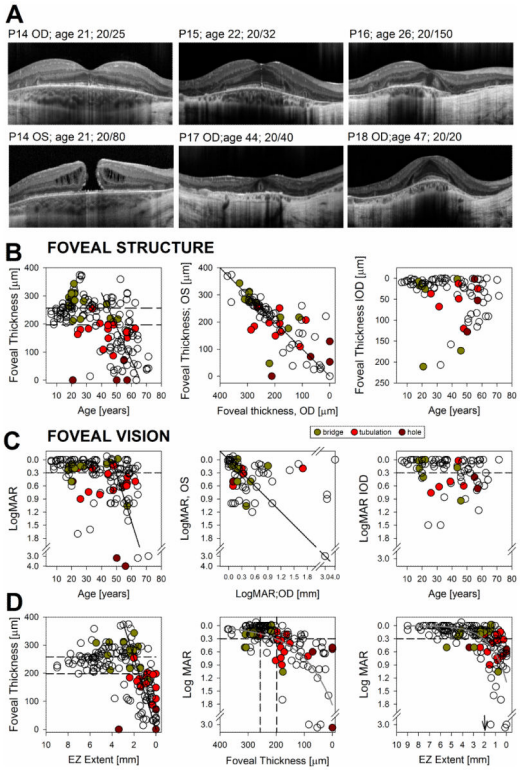

FIGURE 4.

Foveal structure and function in CHM. **A.** SD-OCT horizontal cross-sections through the fovea in patients with CHM. Patients illustrate stages or orderly progression to end stage foveal thinning (top panels) similar to examples shown in Fig. 1 and snapshots of less frequent foveal changes that depart from the norm (*bottom panels*) in this large cross-sectional group of patients with CHM. **B,C** Foveal thickness **(B)** and visual acuity **(C)** plotted as a function of age (left panels), as values from the right eye plotted against the contralateral eye (*middle panels*) and as interocular differences (*right panels*) graphed as a function of age for both foveal thickness and visual acuity. Solid black lines are the manual linear fit to the data for ages >40 years (*left panels*) or equality line (*center panels*). Dashed lines represent normal limits (mean ± 2SD) for foveal thickness and 0.3 LogMAR (20/40) for visual acuity. Occurrence of foveal remodeling with the presence of intraretinal bridges or tracks, of foveal outer retina tubulations and of macular hole are denoted in each graph following legend. **D.** Foveal thickness plotted as a function of EZ lateral extent (*left panels*) and LogMAR plotted independently against these two variables (*middle and right panels*). Dashed lines are as in (B, C). Gray smooth curves are overlaid on data to better visualize the relationships. Black line (*left panel*) is a manual linear fit to the region of faster VA change as a function of EZ extent. Vertical arrow (*right panel*) points to the EZ extent where VA drops below the 0.3 LogMAR for most eyes.

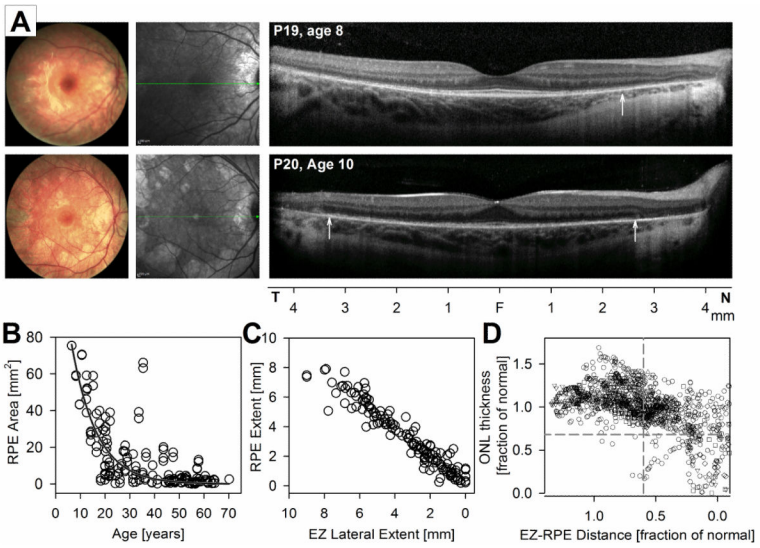

FIGURE 5.

Earliest structural change in CHM. **A.** Color fundus photography (*left panels*), NIR-REF en-face imaging (*middle panels*) and horizontal 9 mm SD-OCT cross-sections through the fovea in two young patients with CHM exemplifying earliest abnormalities. Vertical arrows on the SD-OCT images point to locations outside of which increased back-scattering from RPE demelanization can be appreciated. **B.** Area of apparent normal pigmentation of the fundus by NIR-REF plotted against age (*left panel*). An exponential decay function (*dark gray trace*) describes the data well. **C.** EZ lateral extent plotted as a function of the lateral extent of RPE with apparently preserved melanization. **D.** ONL thickness as a function of EZ-to-RPE distance. Values are specified as a fraction of the mean normal value for each retinal location. Dashed lines are the lower limit (normal mean minus 2SD) for each parameter.

Table 1

Association of OCT parameters and visual acuity with age in patients with choroideremia.

Parameter*	Linear slope for change per year (SE)*				Mean (SE) by age group*			
	All ages	<20 y	20-40 y	>40 y	All ages	<20 y	20-40 y	>40 y
Foveal thickness	−3.0 (0.4)	2.9 (1.4)	−2.0 (1.6)	−3.5 (1.3)	203.3 (6.8)	243.5 (6.2)	256. 8 (10.4)	145.7 (12.4)
P-value†	<0.001	0.04	0.20	0.009				
P-value††			0.06	0.03			0.27	<0.001
ONL extent	−98.8 (8.4)	−15.1 (39.6)	−102.8 (44.7)	−71.2 (36.5)	5688.4 (183.3)	7986.0 (163.8)	6781.8 (284.5)	3967.8 (267.6)
P-value†	<0.001	0.70	0.02	0.05				
P-value††			0.22	0.36			<0.001	<0.001
EZ extent	−94.6 (8.9)	−283.1 (84.2)	−52.1 (38.8)	−4.4 (23.9)	2775.2 (170.5)	5954.6 (407.6)	3339.8 (268.0)	1196.2 (171.5)
P-value†	<0.001	<0.001	0.18	0.85				
P-value††			0.04	0.02			<0.001	<0.001
RPE extent	−95.2 (8.0)	−268.2 (66.7)	−46.2 (35.9)	−16.2 (22.4)	2611.6 (164.9)	5866.0 (350.8)	3211.1 (244.0)	1059.4 (168.3)
P-value†	<0.001	<0.001	0.20	0.47				
P-value††			0.03	0.02			<0.001	<0.001
RPE area	−0.7 (0.1)	−4.0 (0.8)	−0.2 (0.4)	−0.1 (0.1)	13.1 (1.3)	41.6 (5.0)	13.1 (2.3)	3.5 (1.0)
P-value†	<0.001	<0.001	0.69	0.63				
P-value††			0.01	0.01			<0.001	<0.001
Visual acuity (LogMAR)	0.02 (0.00)	0.01 (0.01)	0.01 (0.01)	0.05 (0.02)	0.4 (0.0)	0.08 (0.02)	0.24 (0.04)	0.68 (0.11)
P-value†	<0.001	0.19	0.32	0.006				
P-value††			0.71	0.09			<0.001	<0.001

*Values for OCT parameters are in microns, μm^2 for area (<20 year old; n=30; 20-40 years old, n=66; >40 years old, n=88, eyes).

**Inter-eye correlation of OCT measurements was accounted for using generalized estimating equations (GEE).

†P-values for slope being different than zero for parameter shown in row immediately above.

††P-values for comparisons of the slopes of each of the two older age groups with those of the youngest (<20 year old) group.

Table 2

Interocular difference (OS-OD) of OCT parameters and visual acuity in patients with CHM.

Parameters*	IOD: Summary Statistics				Mean IOD (SD) byAge			
	Mean (SD)	95% Limits of agreement	Intra-class correlation (95% CI)	P-value**	<20 y*	20-40 y*	>40 y*	Linear regression slope with age (SE)
Foveal thickness	4.1 (64.5)	−122, 131	0.75 (0.64, 0.83)	0.56	−2.9 (12.8)	11.1 (63.1)	0.9 (77.0)	0.14 (0.39)
ONL extent:								
Total	5.2 (1847.4)	−3616, 3626	0.71 (0.60, 0.80)	0.98	−3.1 (447.5)	−110.1 (1567.8)	105.8 (2357.5)	3.65 (11.35)
Temporal	49.2 (1243.4)	−2388, 2486	0.63 (0.48, 0.74)	0.71	25.8 (310.7)	36.0 (1182.9)	69.4 (1511.4)	2.10 (7.64)
Nasal	44.0 (950.2)	−1906, 1818	0.70 (0.58, 0.79)	0.67	−28.9 (333.8)	−146.0 (964.3)	36.4 (1097.1)	1.55 (5.84)
EZ extent:								
Total	284.6 (1211.3)	−2090, 2659	0.85 (0.79, 0.90)	0.03	167.4 (883.5)	406.2 (1386.6)	229.6 (1181.5)	0.78 (7.34)
Temporal	215.2 (978.7)	−1703, 2134	0.73 (0.62, 0.82)	0.04	49.1 (774.9)	228.4 (1049.5)	265.4 (1001.5)	5.10 (5.91)
Nasal	69.3 (698.0)	−1299, 1437	0.79 (0.70, 0.86)	0.35	118.3 (732.0)	177.8 (815.4)	−35.8 (574.9)	−4.32 (4.21)
RPE extent	243.0 (1141.6)	−1995, 2481	0.86 (0.8, 0.9)	0.05	398.5 (768.0)	405.8 (1298.6)	71.7 (1123.3)	−8.16 (6.73)
RPE area	0.8 (5.2)	−9.4, 11.0	0.96 (0.9, 1.0)	0.15	0.6 (7.0)	0.9 (4.7)	0.8 (5.1)	0.01 (0.03)
Visual acuity (LogMAR)	−0.1 (0.8)	−1.6, 1.4	0.33 (0.1, 0.5)	0.46	0.0 (0.1)	−0.1 (0.4)	−0.1 (1.1)	−0.002 (0.005)

*Values for OCT parameters are in microns, μm^2 for area (<20 year old; n=30; 20-40 years old, n=66; >40 years old, n=88, eyes; n=97 including patients without OCT but with VA measures); mean for parameter (SD).

**P-value for testing inter-ocular difference is different from 0 or not.